


Please cite the Published Version

Samir, Ahmed, Elsayed, Mohamed, El-Banna, Ahmad A Aziz, Ansari, Imran Shafique, Rabie, Khaled  and Elhalawany, Basem M (2022) Performance analysis of dual-hop hybrid RF-UOWC NOMA systems. *Sensors*, 22 (12). 4521 ISSN 1424-8220

DOI: <https://doi.org/10.3390/s22124521>

Publisher: MDPI

Version: Published Version

Downloaded from: <https://e-space.mmu.ac.uk/632928/>

Usage rights:  [Creative Commons: Attribution 4.0](https://creativecommons.org/licenses/by/4.0/)

Additional Information: This is an open access article which originally appeared in *Sensors*, published by MDPI

Enquiries:

If you have questions about this document, contact openresearch@mmu.ac.uk. Please include the URL of the record in e-space. If you believe that your, or a third party's rights have been compromised through this document please see our Take Down policy (available from <https://www.mmu.ac.uk/library/using-the-library/policies-and-guidelines>)

Article

Performance Analysis of Dual-Hop Hybrid RF-UOWC NOMA Systems

Ahmed Samir ¹, Mohamed Elsayed ¹, Ahmad A. Aziz El-Banna ¹, Imran Shafique Ansari ²,
Khaled Rabie ^{3,4,*} and Basem M. ElHalawany ¹

¹ Faculty of Engineering at Shoubra, Benha University, Cairo 13511, Egypt; ahmed.saied@feng.bu.edu.eg (A.S.); mohamed.elsayed@feng.bu.edu.eg (M.E.); ahmad.elbanna@feng.bu.edu.eg (A.A.A.E.-B.); basem.mamdoh@feng.bu.edu.eg (B.M.E.)

² James Watt School of Engineering, University of Glasgow, Glasgow G12 8QQ, UK; imran.ansari@glasgow.ac.uk

³ Department of Engineering, Manchester Metropolitan University, Manchester M1 5GF, UK

⁴ Department of Electrical and Electronic Engineering, University of Johannesburg, Johannesburg 2028, South Africa

* Correspondence: k.rabie@mmu.ac.uk

Abstract: The hybrid combination between underwater optical wireless communication (UOWC) and radio frequency (RF) is a vital demand for enabling communication through the air–water boundary. On the other hand, non-orthogonal multiple access (NOMA) is a key technology for enhancing system performance in terms of spectral efficiency. In this paper, we propose a downlink NOMA-based dual-hop hybrid RF-UOWC with decode and forward (DF) relaying. The UOWC channels are characterized by exponential-generalized Gamma (EGG) fading, while the RF channel is characterized by Rayleigh fading. Exact closed-form expressions of outage probabilities and approximated closed-form expressions of ergodic capacities are derived, for each NOMA individual user and the overall system as well, under the practical assumption of imperfect successive interference cancellation (SIC). These expressions are then verified via Monte-Carlo simulation for various underwater scenarios. To gain more insight into the system performance, we analyzed the asymptotic outage probabilities and the diversity order. Moreover, we formulated and solved a power allocation optimization problem to obtain an outage-optimal performance. For the sake of comparison and to highlight the achievable gain, the system performance is compared against a benchmark orthogonal multiple access (OMA)-based system.

Keywords: hybrid RF-UOWC; exponential-generalized Gamma; non-orthogonal multiple access; outage probability; optimal power allocation



Citation: Samir, A.; Elsayed, M.; El-Banna, A.A.A.; Shafique Ansari, I.; Rabie, K.; ElHalawany, B.M. Performance Analysis of Dual-Hop Hybrid RF-UOWC NOMA Systems. *Sensors* **2022**, *22*, 4521. <https://doi.org/10.3390/s22124521>

Academic Editor: Joel J. P. C. Rodrigues

Received: 22 May 2022

Accepted: 9 June 2022

Published: 15 June 2022

Publisher's Note: MDPI stays neutral with regard to jurisdictional claims in published maps and institutional affiliations.



Copyright: © 2022 by the authors. Licensee MDPI, Basel, Switzerland. This article is an open access article distributed under the terms and conditions of the Creative Commons Attribution (CC BY) license (<https://creativecommons.org/licenses/by/4.0/>).

1. Introduction

Underwater optical wireless communication (UOWC) has received substantial research interest as an efficient transmission technology for a wide range of underwater applications such as surveillance and oceanic monitoring. Many wireless data transmission techniques faced limitations while communicating underwater, including acoustic waves and radio-frequency (RF) signals. An acoustic-based underwater communication has many drawbacks such as high latency, low data rates, and high attenuation. The situation was not much different when using RF in underwater communication scenarios [1,2]. An acoustic-based underwater communication has many drawbacks such as high latency, low data rates, high bit error rates, and high attenuation. In addition, it severely suffers from malicious attacks. This is due to the fact that acoustic communication channels are uniquely designed for networks used on land; they require more sophisticated security mechanisms [3]. The situation was not much different when using RF in underwater communication scenarios [1]. The underwater RF communications suffers from high power

consumption, high latency, and incompatibility between high speed and long distance. The appropriate alternative to overcome these drawbacks was to go to the use of optical waves to communicate underwater due to its advantages over its counterparts such as low latency, high data rate, and high security when operating in the wavelength range of 450 nm to 550 nm [4–6]. Despite these advantages, the UOWC system suffers from harsh turbulence that prompted the researchers to search for a statistical distribution model to effectively describe the underwater turbulence. In [5], a unified exponential-generalized Gamma (EGG) model that perfectly characterizes underwater channel fading was experimentally derived.

Based on the aforementioned defects resulting from the use of RF in underwater communication, the communication between the on-land and the underwater end terminals was not applicable. Therefore, the integration between RF and UOWC communication systems via relay has become indispensable [7–12]. In [7,8], the authors measured the performance of a mixed RF-UOWC transmission systems in terms of outage probability (OP), average bit error rate, and ergodic capacity (EC) for different systems models. In [9,10], the authors measured the secrecy performance of a mixed RF-UOWC system where an eavesdropper tried to intercept RF communications. The authors in [11] study the performance of a dual-hop RF-UOWC transmission system in terms of OP and bit error rate under both fixed and variable gain relaying schemes in which different detection techniques are derived. The performance analysis of a decode-and-forward (DF) based triple hop radio frequency free space optical communication-underwater optical communication (RF-FSO-UWOC) system was discussed with closed-form expressions for OP and bit-error-rate in [12].

NOMA is a spectrum access technique that has an improving impact on the spectrum efficiency of communication systems, which is considered an optimal solution for underwater internet of things (UIoT) for enabling the communication of a higher number of underwater sensors. NOMA enables simultaneous transmission of multiplexed user data using the same resources (time/frequency/code). Power domain (PD) NOMA is the most common type of NOMA, where the multiplexing is performed by assigning different power levels for the multiplexed messages based on the power allocation factor parameter at the transmitter, while the receiver needs to perform successive interference cancellation (SIC) operation to separate the messages [13–15]. Authors in [16–18] investigated the performance of NOMA assisted underwater optical communication system in terms of coverage probability and system OP. In [15], the authors considered a NOMA-based dual-hop hybrid RF-power line communication system in terms of OP and EC. Additionally, they proved the superiority of NOMA-based system over the OMA-based one.

Hybrid communication systems, where transmission propagates through different environments, are currently attracting a lot of attention. In this paper, to enhance the spectral efficiency, we propose a downlink NOMA-based dual-hop hybrid RF-UOWC system, where the source exploits NOMA to convey two messages intended for two underwater destinations in presence of imperfect SIC. To the best of our knowledge, none of the previous work in the literature has studied hybrid RF-underwater based on NOMA as a spectrum access technique. The authors in [15] have investigated the performance of a wireless/power-line communication system, while our work investigates another hybrid system where the relay works as an intermediate node between wireless and underwater mediums. There are a lot of differences between them in terms of the field of application of the two systems. Our proposed system can find applications in many underwater applications, such as offshore oil field exploration, oceanic monitoring, and data collection. On the other hand, the system in [15] may find applications in situations where the signals suffer from penetration loss within buildings and factories. In [15], the PLC link was assumed to undergo lognormal distribution with Bernoulli Gaussian noise, including both background and impulsive noise components, while this work investigated UOWC channels that are characterized by EGG fading with AWGN.

The main contributions of this paper can be summarized as follows. (1) We derived a new closed-form and asymptotic expressions for the OPs and EC, assuming that the

wireless channel is characterized by Rayleigh fading with an additive white Gaussian noise (AWGN) and the UOWC links are characterized by EGG fading with AWGN. (2) We analyzed the diversity order of the OPs. (3) We proposed and solved a power allocation optimization problem to obtain an outage-optimal power allocation factor. (4) We validated the analytical derivations through Monte-Carlo simulations for varying underwater scenarios of air bubbles level (BL) under thermally uniform and temperature gradient UOWC channels, then we analyzed the impact of system parameters on the system performance. (5) Finally, we carried out a comparison between the proposed system with an OMA-based benchmark system.

The rest of the paper is organized as follows, the system model is introduced in Section 2. The performance of the considered system is analytically evaluated by deriving the OPs and ECs in Sections 3 and 4, respectively. The proposed power allocation algorithm is provided in Section 5. Analytical and simulation results are discussed and compared with a benchmark system in Section 6. Finally, conclusions are provided in Section 7.

2. System Model

In this paper, we propose a downlink NOMA-based dual-hop hybrid RF-UOWC system depicted in Figure 1, where the source (S) is equipped with an RF interface that aims to communicate with two destinations (D_1 and D_2) equipped with UOWC interface via an intermediate decode and forward relay (R). The relay has an RF interface to receive from S and then transmit to D_1 and D_2 through the UOWC interface, where D_1 is the far or weak user and D_2 is the near or strong user. Such a scenario can find applications in many areas in the UIoT [19] (e.g., offshore oil field exploration, oceanic monitoring, and data collection). The S - R channel (h_w) is assumed to be a RF channel characterized by Rayleigh fading with AWGN and the R - D_i channels (h_i) are assumed to be UOWC channels characterized by EGG fading with AWGN, where $i \in \{1, 2\}$.

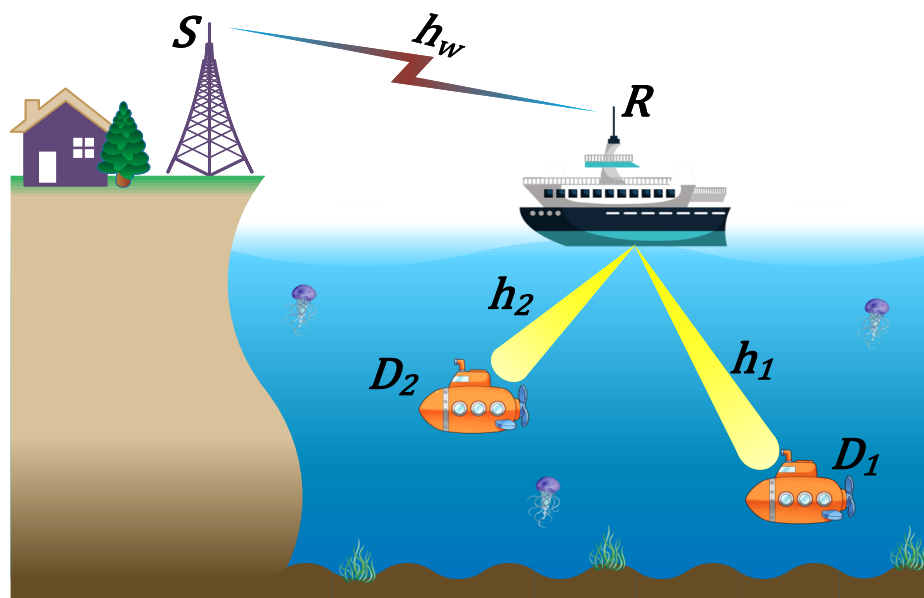


Figure 1. Downlink NOMA-based hybrid RF-UOWC system model.

For the sake of improving the spectral efficiency, we assume that S and R adopt PD-NOMA for multiplexing their messages. The communication is initiated at S by multiplexing the two messages x_1 and x_2 intended for D_1 and D_2 , respectively. The S -to- R message is $x_S = \sqrt{a_1 P_S} x_1 + \sqrt{a_2 P_S} x_2$, where P_S is the total transmitted power at S and a_i is the NOMA power allocation factor for D_i at S . Without loss of generality, we assume that $a_1 > a_2$ and $a_1 + a_2 = 1$. The received message at R through the RF link is $y_R = h_w d^{\frac{-\alpha}{2}} x_S + n_\omega$, where the expectation of RF channels gain is $E[|h_w|^2] = 1$, d is the

S-to-R link distance, v is the RF channel path-loss exponent, and n_ω represents AWGN with $n_\omega \sim \mathcal{CN}(0, \sigma_\omega^2)$. Utilizing NOMA concept, R decodes x_1 first, then applies the SIC operation, which is assumed to be imperfect, to decode x_2 . So, the signal-to-interference-plus noise ratios (SINRs) for decoding x_1 and x_2 are expressed as $\gamma_R^1 = \frac{a_1 \rho_s d^{-v} |h_w|^2}{a_2 \rho_s d^{-v} |h_w|^2 + 1}$ and $\gamma_R^2 = \frac{a_2 \rho_s d^{-v} |h_w|^2}{a_1 \rho_s \eta d^{-v} |h_w|^2 + 1}$, respectively, where $\rho_s = P_S/\sigma_\omega^2$, and $0 \leq \eta \leq 1$ is the residual power factor of the imperfect SIC.

In the second phase, R retransmits the received messages over the UOWC channels that are characterized by independent but not necessarily identical mixture EGG distribution [5]. The relay multiplexes the detected messages using PD-NOMA again, such that $x_R = \sqrt{b_1 P_R} x_1 + \sqrt{b_2 P_R} x_2$, where P_R is the total transmitted power at R and b_i is the NOMA power allocation factor for D_i at R . Without loss of generality, $b_1 > b_2$ and $b_1 + b_2 = 1$. The received message at D_1 through the UOWC link h_1 is $y_{D1} = \varepsilon h_1 x_R + n_u$, where h_1 is the EEG fading of UOWC channel from R -to- D_1 with expectation $E[|h_1|^2] = 1$, ε is responsivity that is considered to be unity, and n_u represents AWGN with $n_u \sim \mathcal{CN}(0, \sigma_u^2)$. Utilizing NOMA concept, D_1 decodes x_1 first. So, the SINR for decoding x_1 at D_1 is expressed as $\gamma_{D1}^1 = \frac{b_1 \rho_R |h_1|^2}{b_2 \rho_R |h_1|^2 + 1}$, where $\rho_R = P_R/\sigma_u^2$.

The received message at D_2 through the UOWC link h_2 is $y_{D2} = \varepsilon h_2 x_R + n_u$, where h_2 is the EEG fading of UOWC channel from R -to- D_2 with expectation $E[|h_2|^2] = 1$. Following the NOMA principle, D_2 decodes x_1 first and then applies the SIC operation, which is assumed to be imperfect, to decode x_2 . So, the SINRs for decoding x_1 and x_2 are expressed as $\gamma_{D2}^1 = \frac{b_1 \rho_R |h_2|^2}{b_2 \rho_R |h_2|^2 + 1}$ and $\gamma_{D2}^2 = \frac{b_2 \rho_R |h_2|^2}{b_1 \rho_R \eta |h_2|^2 + 1}$.

Channels Distributions: We assume that the UOWC links h_1 and h_2 are characterized by the EGG distribution [5], which models the underwater turbulence fading resulting from air bubbles and gradient of temperature in an effective manner. EGG is a weighted combination of the exponential and generalized Gamma distributions, it effectively matches the experimental results obtained under different scenarios of channel impairments of UOWC. A closed-form expression for the cumulative distribution function (CDF) of EGG distribution is given as [5]

$$F_{|h_i|^2}(x) = w G_{1,2}^{1,1} \left(\frac{1}{\lambda} \left(\frac{x}{\mu_r} \right)^{\frac{1}{r}} \middle| \begin{matrix} 1 \\ 1, 0 \end{matrix} \right) + \frac{1-w}{\Gamma(a)} G_{1,2}^{1,1} \left(\frac{1}{b^c} \left(\frac{x}{\mu_r} \right)^{\frac{c}{r}} \middle| \begin{matrix} 1 \\ a, 0 \end{matrix} \right), \quad (1)$$

where $0 < w < 1$ represents the mixture ratio between exponential and generalized Gamma distributions, λ is the exponential distribution scale parameter of the exponential distribution, (a, b, c) are the parameters associated with generalized Gamma distribution, and $G_{m,n}^{p,q}(\cdot)$ is the Meijer-G function [20]. According to the receiver detection method, heterodyne detection ($r = 1$) or intensity modulation/direct detection (IM/DD) ($r = 2$), the electrical signal to noise ratio (SNR) is

$$\mu_{ri} = \begin{cases} \Omega_{xi} & r = 1 \\ \frac{\Omega_{xi}}{2w\lambda^2 + b^2(1-w)\Gamma(a + \frac{c}{r})/\Gamma(a)} & r = 2 \end{cases}, \quad (2)$$

where Ω_{xi} is the average SNR of the UOWC links. We assume that $\Omega_{x1} = \Omega_{x2} = \Omega_x$, thus $\mu_{r1} = \mu_{r2} = \mu_r$. The values of (w, λ, a, b, c) for different scenarios of air bubbles under thermally uniform and gradient-based UOWC channels are experimentally obtained in [5]

(Tables 1 and 2). Finally, the RF-links h_w undergo a Rayleigh fading with AWGN noise, therefore $|h_i|^2$ follows an exponential distribution whose CDF is given as

$$F_{|h_w|^2}(x) = 1 - e^{-x}. \quad (3)$$

Table 1. EGG parameters for temperature gradient water [5].

<i>BL</i> (L/min)	<i>TG</i> C·cm ⁻¹	<i>w</i>	λ	<i>a</i>	<i>b</i>	<i>c</i>
2.4	0.05	0.2130	0.3291	1.4299	1.1817	17.1984
2.4	0.15	0.1807	0.1641	0.2334	1.4201	22.5924
4.7	0.1	0.4539	0.2744	0.3008	1.7053	54.1422

Table 2. EGG parameters for thermally uniform salty water [5].

<i>BL</i> (L/min)	<i>w</i>	λ	<i>a</i>	<i>b</i>	<i>c</i>
2.4	0.1770	0.4687	0.7736	1.1372	49.1773
4.7	0.2064	0.3953	0.5307	1.2154	35.7368

3. Outage Probability Analysis

In this section, the system performance analysis in terms of OPs is presented. The OPs are defined as the probability that the received SINR falls below a certain threshold limit. We derived closed-form expressions for the outage at each destination as well as the overall system outage. Then, we derive an asymptotic expression for each of them at a high SNR regime. To gain more insight into the system performance, the outage diversity order is further derived.

3.1. Outage Probability OP_1

The outage event of D_1 , OP_1 , occurs if R or D_1 fails to decode x_1 , which can be formulated as

$$\begin{aligned} OP_1 &= 1 - Pr(\gamma_R^1 > \gamma_1, \gamma_{D1}^1 > \gamma_1) \\ &\stackrel{(a)}{=} 1 - Pr(|h_w|^2 > \frac{\tau_1}{\rho_s d^{-\nu}}) \times Pr(|h_1|^2 > \frac{\beta_1}{\rho_R}), \end{aligned} \quad (4)$$

where (a) stems from the independence between h_w and h_1 , $\gamma_1 = 2^{R_1} - 1$ with R_1 as the target data rate of x_1 , $\tau_1 = \gamma_1 / (a_1 - a_2 \gamma_1)$ under condition that $a_1 > a_2 \gamma_1$ or $a_1 > \gamma_1 / (1 + \gamma_1)$, and similarly $\beta_1 = \gamma_1 / (b_1 - b_2 \gamma_1)$ under condition that $b_1 > b_2 \gamma_1$ or $b_1 > \gamma_1 / (1 + \gamma_1)$. With the aid of CDFs in (1) and (3), we obtain a closed-form expression of OP_1 as in (5).

$$OP_1 = 1 - e^{\frac{-\tau_1}{\rho_s d^{-\nu}}} \left(1 - w G_{1,2}^{1,1} \left(\frac{1}{\lambda} \left(\frac{\beta_1}{\rho_R \mu_r} \right)^{\frac{1}{r}} \mid \frac{1}{1,0} \right) - \frac{1-w}{\Gamma(a)} G_{1,2}^{1,1} \left(\frac{1}{b^c} \left(\frac{\beta_1}{\rho_R \mu_r} \right)^{\frac{c}{r}} \mid \frac{1}{a,0} \right) \right). \quad (5)$$

3.2. Outage Probability OP_2

The outage OP_2 occurs if R or D_2 fails to decode x_1 or x_2 ; this is due to NOMA SIC concept that involves receiving x_1 and cancels it before receiving x_2 . It is formulated as

$$\begin{aligned} OP_2 &= 1 - Pr(\gamma_R^1 > \gamma_1, \gamma_R^2 > \gamma_2, \gamma_{D2}^1 > \gamma_1, \gamma_{D2}^2 > \gamma_2) \\ &\stackrel{(b)}{=} 1 - Pr(|h_w|^2 > \frac{\tau_1}{\rho_s d^{-\nu}}, |h_w|^2 > \frac{\tau_2}{\rho_s d^{-\nu}}) \times Pr(|h_2|^2 > \frac{\beta_1}{\rho_R}, |h_2|^2 > \frac{\beta_2}{\rho_R}) \\ &= 1 - Pr(|h_w|^2 > \frac{\tau}{\rho_s d^{-\nu}}) \times Pr(|h_2|^2 > \frac{\beta}{\rho_R}), \end{aligned} \quad (6)$$

where (b) stems from the independence between h_w and h_2 , $\gamma_2 = 2^{R_2} - 1$ with R_2 is the target data rate of x_2 , $\tau_2 = \gamma_2/(a_2 - a_1\eta\gamma_2)$ under condition that $a_2 > a_1\eta\gamma_2$ or $a_1 < 1/(1 + \eta\gamma_2)$, similarly $\beta_2 = \gamma_2/(b_2 - b_1\eta\gamma_2)$ under condition that $b_2 > b_1\eta\gamma_2$ or $b_1 < 1/(1 + \eta\gamma_2)$, $\tau = \max(\tau_1, \tau_2)$, and $\beta = \max(\beta_1, \beta_2)$. With the aid of CDFs in (1) and (3), we obtain a closed-form expression of OP_2 as in (7).

$$OP_2 = 1 - e^{\frac{-\tau}{\rho_s d^{-v}}} \left(1 - w G_{1,2}^{1,1} \left(\frac{1}{\lambda} \left(\frac{\beta}{\rho_R \mu_r} \right)^{\frac{1}{r}} \mid 1, 0 \right) - \frac{1-w}{\Gamma(a)} G_{1,2}^{1,1} \left(\frac{1}{b^c} \left(\frac{\beta}{\rho_R \mu_r} \right)^{\frac{c}{r}} \mid a, 0 \right) \right). \quad (7)$$

3.3. System Outage Probability OP_{sys}

The total system outage OP_{sys} occurs if R or D_2 fails to decode any of the two messages or D_1 fails to decode x_1 . It is formulated as

$$\begin{aligned} OP_{sys} &= 1 - Pr(\gamma_R^1 > \gamma_1, \gamma_R^2 > \gamma_2, \gamma_{D2}^1 > \gamma_1, \gamma_{D2}^2 > \gamma_2, \gamma_{D1}^1 > \gamma_1) \\ &\stackrel{(c)}{=} 1 - Pr(|h_w|^2 > \frac{\tau_1}{\rho_s d^{-v}}, |h_w|^2 > \frac{\tau_2}{\rho_s d^{-v}}) \\ &\quad \times Pr(|h_2|^2 > \frac{\beta_1}{\rho_R}, |h_2|^2 > \frac{\beta_2}{\rho_R}) \times Pr(|h_1|^2 > \frac{\beta_1}{\rho_R}) \\ &= 1 - Pr(|h_w|^2 > \frac{\tau}{\rho_s d^{-v}}) \times Pr(|h_2|^2 > \frac{\beta}{\rho_R}) \times Pr(|h_1|^2 > \frac{\beta_1}{\rho_R}), \end{aligned} \quad (8)$$

where (c) stems from the independence between h_w , h_1 , and h_2 . With the aid of CDFs in (1) and (3), we obtain a closed-form expression of OP_2 as in (9).

$$\begin{aligned} OP_{sys} &= 1 - e^{\frac{-\tau}{\rho_s d^{-v}}} \left(1 - w G_{1,2}^{1,1} \left(\frac{1}{\lambda} \left(\frac{\beta}{\rho_R \mu_r} \right)^{\frac{1}{r}} \mid 1, 0 \right) - \frac{1-w}{\Gamma(a)} G_{1,2}^{1,1} \left(\frac{1}{b^c} \left(\frac{\beta}{\rho_R \mu_r} \right)^{\frac{c}{r}} \mid a, 0 \right) \right) \\ &\quad \times \left(1 - w G_{1,2}^{1,1} \left(\frac{1}{\lambda} \left(\frac{\beta_1}{\rho_R \mu_r} \right)^{\frac{1}{r}} \mid 1, 0 \right) - \frac{1-w}{\Gamma(a)} G_{1,2}^{1,1} \left(\frac{1}{b^c} \left(\frac{\beta_1}{\rho_R \mu_r} \right)^{\frac{c}{r}} \mid a, 0 \right) \right). \end{aligned} \quad (9)$$

3.4. Asymptotic Outage Probability

A deep insight on the system performance under high SNRs regime is obtained through the derivation of the asymptotic outage probabilities. A tight asymptotic expression for the CDF of the exponential and EGG distributions at high SNR are [5]

$$F_{|h_w|^2}(x) \simeq x, \quad (10)$$

$$F_{|h_i|^2}(x) \simeq \frac{w}{\lambda} \left(\frac{x}{\mu_r} \right)^{\frac{1}{r}} + \frac{1-w}{\Gamma(a+1)} \left(\frac{x}{b^r \mu_r} \right)^{\frac{ac}{r}}. \quad (11)$$

Based on (10) and (11), we derive asymptotic expressions for OP_1 , OP_2 , and OP_{sys} as

$$OP_1^\infty \simeq 1 - \left(1 - \frac{\tau_1}{\rho_s d^{-v}} \right) \left(1 - \frac{w}{\lambda} \left(\frac{\beta_1}{\rho_R \mu_r} \right)^{\frac{1}{r}} - \frac{1-w}{\Gamma(a+1)} \left(\frac{\beta_1}{b^r \rho_R \mu_r} \right)^{\frac{ac}{r}} \right), \quad (12)$$

$$OP_2^\infty \simeq 1 - \left(1 - \frac{\tau}{\rho_s d^{-v}} \right) \left(1 - \frac{w}{\lambda} \left(\frac{\beta}{\rho_R \mu_r} \right)^{\frac{1}{r}} - \frac{1-w}{\Gamma(a+1)} \left(\frac{\beta}{b^r \rho_R \mu_r} \right)^{\frac{ac}{r}} \right), \quad (13)$$

$$\begin{aligned} OP_{sys}^\infty &\simeq 1 - \left(1 - \frac{\tau}{\rho_s d^{-v}} \right) \left(1 - \frac{w}{\lambda} \left(\frac{\beta}{\rho_R \mu_r} \right)^{\frac{1}{r}} - \frac{1-w}{\Gamma(a+1)} \left(\frac{\beta}{b^r \rho_R \mu_r} \right)^{\frac{ac}{r}} \right) \\ &\quad \times \left(1 - \frac{w}{\lambda} \left(\frac{\beta_1}{\rho_R \mu_r} \right)^{\frac{1}{r}} - \frac{1-w}{\Gamma(a+1)} \left(\frac{\beta_1}{b^r \rho_R \mu_r} \right)^{\frac{ac}{r}} \right). \end{aligned} \quad (14)$$

3.5. Diversity Order

To gain more insight, we study the achievable diversity order (DO) of the obtained OPs. DO is the slope of OP_l where $l \in \{1, 2, sys\}$. According to [21], we can calculate diversity order as $DO_l = -\lim_{\rho \rightarrow \infty} (\log(OP_l) / \log(\rho))$. It is clear from (12)–(14) that $DO_l = \min(1, \frac{1}{r})$. As $\frac{ac}{r} \gg 1$ in all scenarios, this result is consistent with the plots in Figure 2.

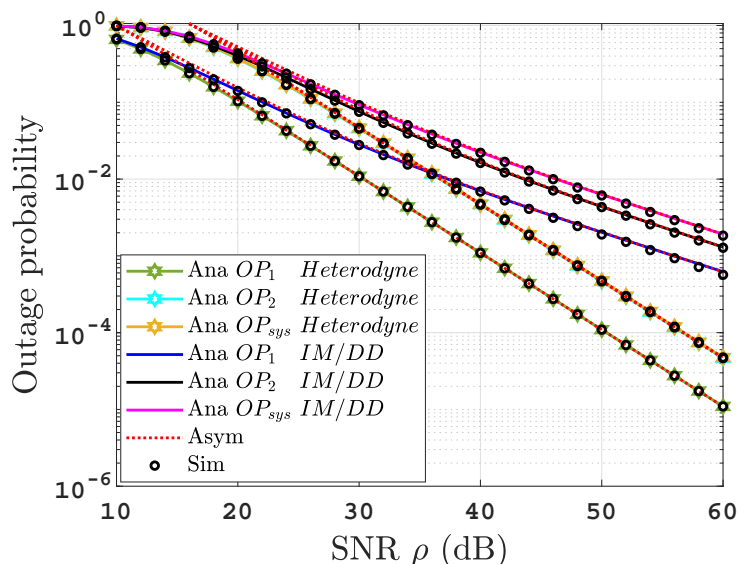


Figure 2. OPs versus SNR for thermally uniform UOWC links for both IM/DD as well as heterodyne detection.

4. Ergodic Capacity Analysis

In this section, we derive an approximated closed-form expression for the ergodic capacity (EC) of the proposed system under the condition $a_i = b_i$. The instantaneous channel capacities for the two messages, C_{x_1}, C_{x_2} , are given by [13,22]

$$\begin{aligned}
 C_{x_1} &= \frac{1}{2} \log_2(1 + \min(\gamma_R^1, \gamma_{D1}^1, \gamma_{D2}^1)) \\
 C_{x_2} &= \frac{1}{2} \log_2(1 + \min(\gamma_R^2, \gamma_{D2}^2)).
 \end{aligned}
 \tag{15}$$

The EC, defined as the expectation of the channel capacity, can be mathematically expressed as [21]

$$EC_{x_i} = \frac{1}{2 \ln 2} \int_{\gamma=0}^{\infty} \frac{1}{1 + \gamma} [1 - F_{\gamma_j}(\gamma)] d\gamma,
 \tag{16}$$

where $j \in \{a, b\}$. The ergodic sum capacity (ESC) can be expressed as

$$ESC = EC_{x_1} + EC_{x_2}.
 \tag{17}$$

In the following subsections, we derive the individual ECs.

4.1. Ergodic Capacity EC_{x_1}

The CDF $F_{\gamma_a}(\gamma)$ is given as

$$\begin{aligned} F_{\gamma_a}(\gamma) &= 1 - \Pr(\gamma_R^1 > \gamma, \gamma_{D1}^1 > \gamma, \gamma_{D2}^1 > \gamma) \\ &\stackrel{(d)}{=} 1 - \Pr(|h_w|^2 > \frac{\gamma}{\rho_s d^{-v}(a_1 - a_2 \gamma)}) \Pr(|h_1|^2 > \frac{\gamma}{\rho_R(a_1 - a_2 \gamma)}) \Pr(|h_2|^2 > \frac{\gamma}{\rho_R(a_1 - a_2 \gamma)}), \end{aligned} \quad (18)$$

where (d) stems from the independence of the channels gain and $0 < \gamma < \frac{a_1}{a_2}$. Then

$$\begin{aligned} EC_{x_1} &= \frac{1}{2\ell n 2} \int_{\gamma=0}^{a_1/a_2} \frac{1}{1+\gamma} (1 - F_{|h_w|^2}(\frac{\gamma}{\rho_s d^{-v}(a_1 - a_2 \gamma)})) \\ &\times (1 - F_{|h_1|^2}(\frac{\gamma}{\rho_R(a_1 - a_2 \gamma)})) (1 - F_{|h_2|^2}(\frac{\gamma}{\rho_R(a_1 - a_2 \gamma)})) d\gamma, \end{aligned} \quad (19)$$

then applying variable transformation of $\tau_a = \gamma/(a_1 - a_2 \gamma)$ and using the exponential distribution CDF in (3) and the tight approximated EGG CDF at high SNR in (11), we can write

$$EC_{x_1} = \frac{1}{2\ell n 2} \int_{\gamma=0}^{\infty} \frac{e^{-\phi_1 \tau_a} (1 - \phi_2 \tau_a^{\frac{1}{r}} - \phi_3 \tau_a^{\frac{ac}{r}})^2}{(1 + \tau_a)(1 + a_2 \tau_a)} d\tau_a, \quad (20)$$

where $\phi_1 = 1/\rho_s d^{-v}$, $\phi_2 = (w/\lambda)(1/\rho_R \mu_r)^{\frac{1}{r}}$, and $\phi_3 = ((1-w)/\Gamma(a+1))(1/b^r \rho_R \mu_r)^{\frac{ac}{r}}$. Using binomial expansion

$$EC_{x_1} = \frac{1}{2\ell n 2} (I_1 - 2\phi_2 I_2 - 2\phi_3 I_3 + \phi_2^2 I_4 + 2\phi_2 \phi_3 I_5 + \phi_3^2 I_6), \quad (21)$$

where

$$\begin{aligned} I_K &= \int_{\gamma=0}^{\infty} \frac{\tau_a^{X_K} e^{-\phi_1 \tau_a} d\tau_a}{(1 + \tau_a)(1 + a_2 \tau_a)} \\ &= \frac{1}{a_1} \int_{\gamma=0}^{\infty} \frac{\tau_a^{X_K} e^{-\phi_1 \tau_a} d\tau_a}{(1 + \tau_a)} - \frac{1}{a_1} \int_{\gamma=0}^{\infty} \frac{\tau_a^{X_K} e^{-\phi_1 \tau_a} d\tau_a}{((1/a_2) + \tau_a)}, \end{aligned} \quad (22)$$

where $K \in [1, 6]$ and X_K is the K^{th} element in the vector $X = [0, (1/r), (ac/r), (2/r), ((1+ac)/r), (2ac/r)]$. Utilizing [23] (Equation 3.383.10), I_K can be expressed as

$$I_K = \frac{1}{a_1} \Gamma(X_K + 1) [(e^{\phi_1} \Gamma(-X_K, \phi_1)) - ((\frac{1}{a_2})^{X_K} e^{\frac{\phi_1}{a_2}} \Gamma(-X_K, \frac{\phi_1}{a_2}))]. \quad (23)$$

Substituting (23) into (21), a closed-form expression of EC_{x_1} is obtained.

4.2. Ergodic Capacity EC_{x_2}

The CDF $F_{\gamma_b}(\gamma)$ is given as

$$\begin{aligned} F_{\gamma_b}(\gamma) &= 1 - \Pr(\gamma_R^2 > \gamma, \gamma_{D2}^2 > \gamma) \\ &\stackrel{(e)}{=} 1 - \Pr(|h_w|^2 > \frac{\gamma}{\rho_s d^{-v}(a_2 - \eta a_1 \gamma)}) \times \Pr(|h_2|^2 > \frac{\gamma}{\rho_R(a_2 - \eta a_1 \gamma)}), \end{aligned} \quad (24)$$

where (e) stems from the independence of the channels gain and $0 < \gamma < \frac{a_2}{a_1 \eta}$. Then

$$EC_{x_2} = \frac{1}{2\ell n 2} \int_{\gamma=0}^{a_2/\eta a_1} \frac{1}{1+\gamma} (1 - F_{|h_w|^2}(\frac{\gamma}{\rho_s d^{-\nu}(a_2 - \eta a_1 \gamma)})) (1 - F_{|h_2|^2}(\frac{\gamma}{\rho_R(a_2 - \eta a_1 \gamma)})) d\gamma, \quad (25)$$

then applying variable transformation of $\tau_b = \gamma/(a_2 - \eta a_1 \gamma)$ and using the Rayleigh CDF (3) and the tight approximated EGG CDF at high SNR (11), we can write

$$\begin{aligned} EC_{x_2} &= \frac{1}{2\ell n 2} \int_{\gamma=0}^{\infty} \frac{e^{-\phi_1 \tau_b} (1 - \phi_2 \tau_b^{\frac{1}{r}} - \phi_3 \tau_b^{\frac{ac}{r}})}{(1 + \eta a_1 \tau_b)(1 + (a_2 + \eta a_1) \tau_b)} d\tau_b \\ &= \frac{1}{2\ell n 2} (J_1 - \phi_2 J_2 - \phi_3 J_3), \end{aligned} \quad (26)$$

where

$$\begin{aligned} J_M &= \int_{\gamma=0}^{\infty} \frac{\tau_b^{Y_M} e^{-\phi_1 \tau_b} d\tau_b}{(1 + \eta a_1 \tau_b)(1 + (a_2 + \eta a_1) \tau_b)} \\ &= \frac{1}{a_2} \int_{\gamma=0}^{\infty} \frac{\tau_b^{Y_M} e^{-\phi_1 \tau_b} d\tau_b}{(\frac{1}{(a_2 + \eta a_1)} + \tau_b)} - \frac{1}{a_2} \int_{\gamma=0}^{\infty} \frac{\tau_b^{Y_M} e^{-\phi_1 \tau_b} d\tau_b}{(\frac{1}{\eta a_1} + \tau_b)}, \end{aligned} \quad (27)$$

where $M \in \{1, 2, 3\}$ and Y_M is the M th element in the vector $Y = [0, (1/r), (ac/r)]$. Using [23] (Equation 3.383.10), J_M can be expressed as

$$J_M = \frac{\Gamma(Y_M + 1)}{a_2} [((\frac{1}{a_2 + \eta a_1})^{Y_M} e^{\frac{\phi_1}{(a_2 + \eta a_1)}} \Gamma(-Y_M, \frac{\phi_1}{(a_2 + \eta a_1)})) - ((\frac{1}{\eta a_1})^{Y_M} e^{\frac{\phi_1}{\eta a_1}} \Gamma(-Y_M, \frac{\phi_1}{\eta a_1}))]. \quad (28)$$

By Substituting (28) into (26), a closed-form expression of EC_{x_2} is obtained.

5. Proposed Power Allocation Algorithm

In this section, we propose a power allocation algorithm for optimizing the system OP under the condition $a_i = b_i$, where $i \in \{1, 2\}$ or equivalently $\tau_i = \beta_i$ and $\tau = \beta$. The proposed optimization problem is expressed as

$$\min_{a_1} OP_{sys} \quad (29a)$$

$$\text{s.t. } \frac{\gamma_1}{1 + \gamma_1} < a_1 < \frac{1}{1 + \eta \gamma_2} \quad (29b)$$

$$a_1 + a_2 = 1. \quad (29c)$$

We provide the following Theorem to solve Problem (29).

Theorem 1. Problem (29) is a convex problem, and the optimal power allocation factor value is $a_1^* = \frac{\gamma_1(1 + \gamma_2)}{\gamma_1 + \gamma_2 + \gamma_1 \gamma_2(1 + \eta)}$.

Proof. See Appendix A. \square

Figure 6 graphically verifies that the obtained result in Theorem 1 is correct. We set $R_1 = 0.5$ and $R_2 = 0.75$ as a test values, which implies that $a_1^* \approx 0.58$ mathematically, which is consistent with the optimal value in Figure 6.

6. Results and Discussion

In this section, we provide a detailed discussion on the derived metrics of the proposed system under varying conditions of air bubbles for both fresh/salty and thermally uniform

waters under heterodyne or IM/DD detection techniques to gain more insight and highlight some conclusions. The correctness of the obtained analysis is verified via a Monte-Carlo simulation with 10^6 samples. Throughout this section, we used the distribution parameters provided in Tables 1 and 2. Unless otherwise mentioned, the system parameters are set to $a_1 = b_1 = 0.7$, $\eta = 0.1$, $R_1 = 0.5$ bits/sec/Hz, and $R_2 = 0.75$ bits/sec/Hz; $d = 0.8$ is the normalized distance with respect to the cell radius, and $v = 2$, $\rho_s = \rho_R = \rho$, and $\Omega_x = 1$. In the following, we denote “Ana” as the analytical result, “Asym” as an asymptotic result, and “Sim” as Monte-Carlo simulation results.

Figure 2 presents the outage probability for the proposed system under uniform temperature salty water for both IM/DD and heterodyne techniques. As expected, it can be deduced that the OPs significantly improve when heterodyne detection is implemented compared to IM/DD. This result is due to the ability of the heterodyne receiver to overcome the UOWC link’s turbulence effects, while this leads to a more complex receiver compared to IM/DD receiver. For example, the OP_{sys} of 10^{-2} is achieved at $\rho = 37$ dB under the heterodyne receiver and $\rho = 46$ dB using the IM/DD receiver. It is remarkable that the analytical and the simulation results are a match, which validates our analytical derivations. Additionally, they match the asymptotic curves at high SNR regime. In addition, to validate the DO derived in Section 3.5, we can observe that for heterodyne detection $r = 1$, the $OP_{sys} = 0.0004747$ at $\rho = 50$ dB and $OP_{sys} = 0.00004747$ at $\rho = 60$ dB; therefore, the OP_{sys} falls with a slope of $\log(0.0004747) - \log(0.00004747) = 1$. Following the same procedure for IM/DD, we can observe that the $OP_{sys} = 0.006119$ at $\rho = 50$ dB while $OP_{sys} = 0.001835$ at $\rho = 60$ dB, so the OP_{sys} falls with a slope of $\log(0.006119) - \log(0.001835) \approx 0.5$. These results are consistent with the diversity order DO_l .

Figure 3 depicts the OPs for the proposed system under uniform temperature salty water with varying air bubbles levels $BL = 2.4$ and $BL = 4.7$ L/min. It is clear that the increase in the level of air bubbles leads to a degradation in the OPs performance. This is due to the rise of the water turbulence. To evaluate the performance of the proposed system in this work, we compared its performance with a benchmark scheme: the OMA-based dual-hop hybrid RF-UOWC system. Figure 3 provides the comparison between the proposed NOMA-based system versus the OMA-based system under the same system settings. According to the figure, the proposed system outperforms the benchmark in terms of OPs performance. This is due to the fact that the NOMA technique is more spectral efficient than the OMA technique.

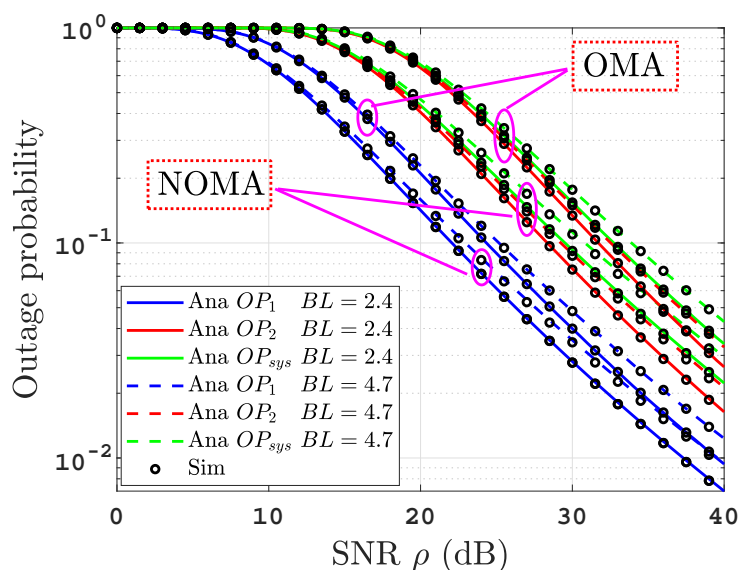


Figure 3. OPs versus SNR for thermally uniform UOWC links for varying air bubbles levels applicable to NOMA and OMA based systems.

Figure 4 illustrates the influence of the residual power factor of imperfect SIC on OPs performance of the proposed system under uniform thermally salty water at $BL = 2.4$ L/min utilizing three varying levels of $\eta = 0, 0.1, 0.2$. We can see that the OPs performance degrades by increasing η while the best performance is achieved with the perfect SIC scenario ($\eta = 0$). This is due to the fact that an increase in η leads to a higher interference level, hence the SINRs γ_R^2 and γ_{D2}^2 decrease while decoding the near user message. However, the SINRs γ_R^1 , γ_{D1}^1 , and γ_{D2}^1 are not affected by changing η .

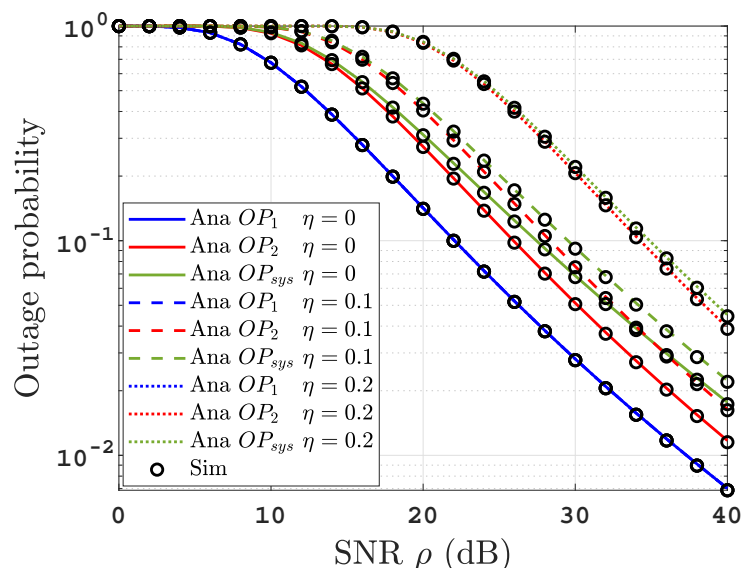


Figure 4. OPs versus SNR for thermally uniform salty UOWC links at $BL = 2.4$ L/min for varying values of η .

Furthermore, Figure 5 depicts the temperature gradient (TG) and air bubbles level effect on the OPs performance. This figure investigated three different scenarios. We set $BL = 2.4$ and $TG = 0.05$ in case1, $BL = 2.4$ and $TG = 0.15$ in case2, and $BL = 4.7$ and $TG = 0.1$ in case3. It is clear that the higher the level of the air bubbles and/or the temperature gradient, the stronger the turbulence, leading to a OPs performance deterioration.

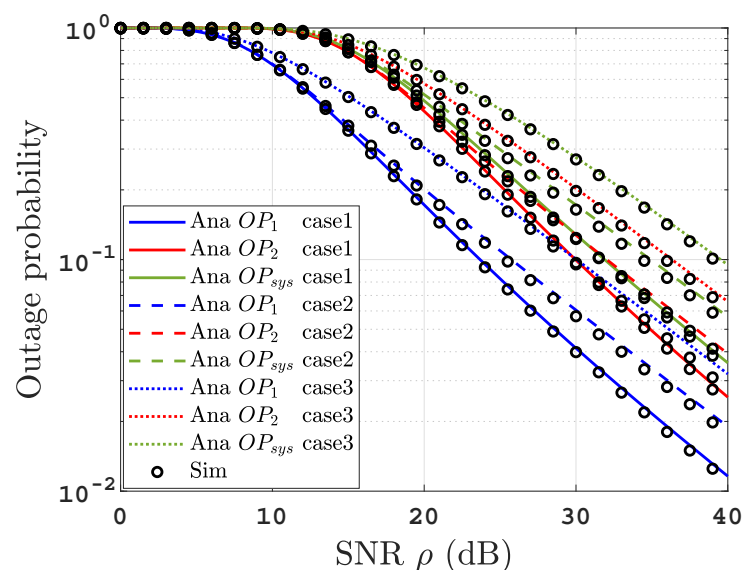


Figure 5. The effect of temperature gradient and air bubbles level on OPs performance.

Figure 6 demonstrates the influence of the power allocation factor $a_1 = b_1$, which varies from 0.5 to 0.99, on the OPs performance with $\rho = 40$ dB in two varying air bubble

levels of $BL = 2.4$ and $BL = 4.7$ L/min. We can observe that the OP_1 enhances with the increase in a_1 due to the increase of its own message power. On the other hand, the OP_2 witnesses an improvement at first with a_1 increase as D_2 needs to decode x_1 first before decoding its own message x_2 . However, with the continuous increase in a_1 , an inflection point is reached since increasing a_1 means decreasing the allocated power for D_2 message ($a_2 = 1 - a_1$) that degrades the OP_2 . Finally, the OP_{sys} follows the same trend as OP_2 with a bit increase. Additionally, this figure graphically proves the convexity of the optimization problem in (29).

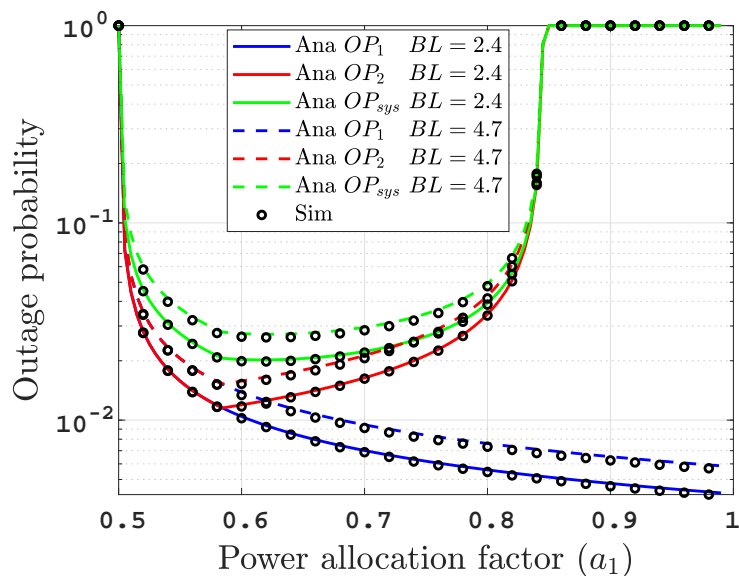


Figure 6. OPs over the entire range of power allocation factor at SNR = 40 dB.

Figure 7 illustrates the influence of the residual power factor of imperfect SIC on ECs performance of the proposed system under uniform thermally salty water at $BL = 2.4$ L/min where $\eta = 0.01$, and 0.05. We can see that the EC_{x_2} and ESC performance degrades by increasing η . This is due to the fact that an increase in η leads to a higher interference level at the decoding process of x_2 . On the other hand, the EC_{x_1} performance is not affected by changing η . The figure also shows a perfect agreement between the simulation and the obtained analytical results at high SNR with a small deviation at low SNR. This deviation is due to the usage of the tight approximated expression for the CDF of the EGG distributions at high SNR.

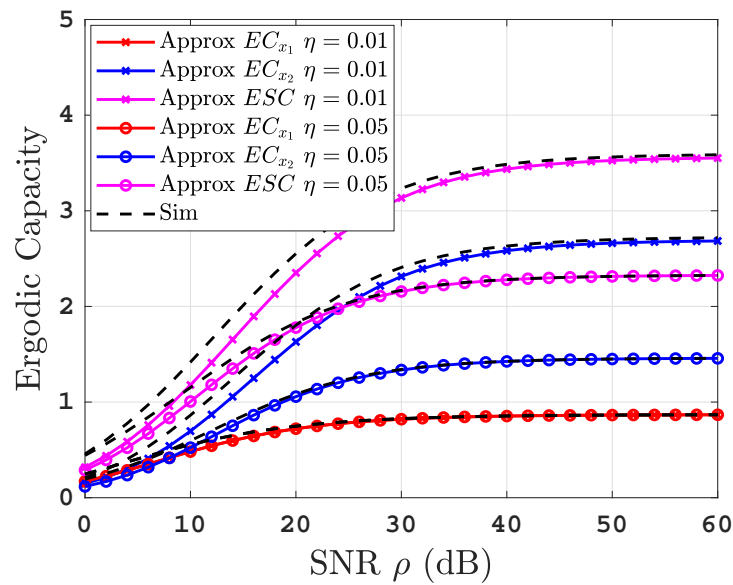


Figure 7. ECs versus SNR for thermally uniform salty UOWC links at $BL = 2.4$ L/min for varying values of η .

Figure 8 illustrates the ECs for the proposed system under uniform temperature salty water with two air bubble levels of $BL = 2.4$ and $BL = 4.7$ L/min. It is clear that the increase in the level of air bubbles leads to a deterioration in the ECs performance; this is due to the increase in water turbulence.

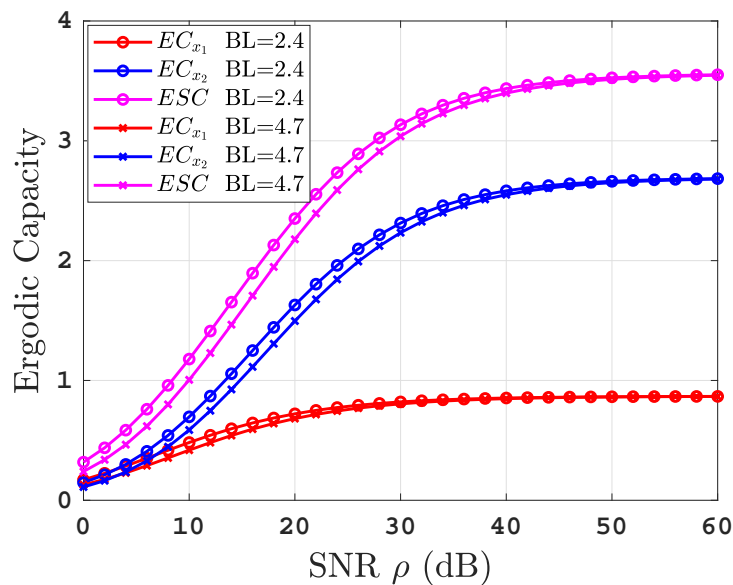


Figure 8. ECs versus SNR for thermally uniform UOWC links for varying air bubbles levels.

Moreover, Figure 9 shows the effect of TG on the ECs performance in salty water under the air bubbles level $BL = 2.4$ L/min. The figure investigated two different values of $TG = 0.05, 0.15$. It is obvious that the higher the level of the temperature gradient, the stronger the turbulence, leading to a ECs performance degradation. From Figures 8 and 9, we can conclude that the effect of the variation in water turbulence (BL, TG) is negligible at the high SNR regime.

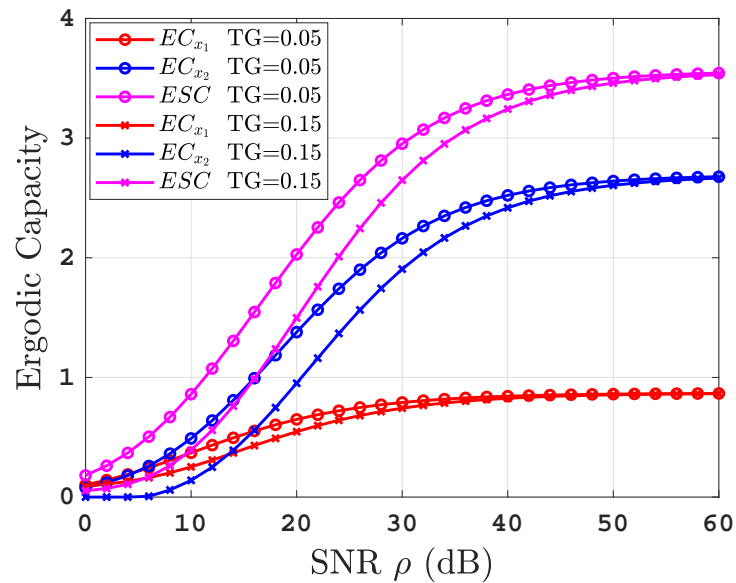


Figure 9. The effect of temperature gradient on ECs performance.

Figure 10 demonstrates the influence of the power allocation factor a_1 , which varies from 0.5 to 0.99, on the ECs performance to gain insight into the effectiveness and the fairness with $\rho = 50$ dB, under uniform temperature salty water with $BL = 2.4$. We can see that EC_{x_1} increases as a_1 increases because the higher power allocation factor means a higher SINRs γ_{R}^1 , γ_{D1}^1 , and γ_{D2}^1 , but EC_{x_2} drops as power allocation factor increases because the SINRs γ_{R}^2 and γ_{D2}^2 degrade. Furthermore, we can see that ESC is approximately constant over the entire range of the power allocation factor, which is owing to the fact that the rate of increase in EC_{x_1} is approximately the same as the rate of decline in EC_{x_2} .

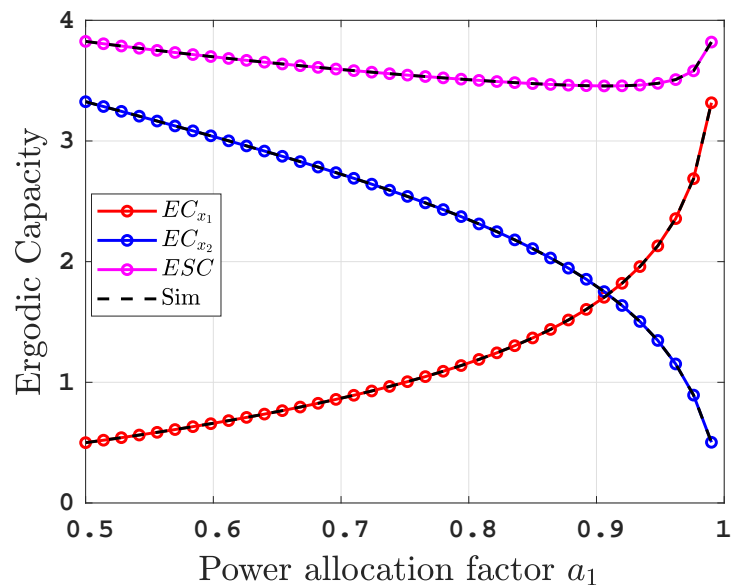


Figure 10. ECs over the entire range of power allocation factor at $\rho = 50$ dB.

7. Conclusions

In this paper, we analyzed the system performance in terms of OP and EC and optimized the OP of a downlink NOMA-based dual-hop hybrid RF-UOWC system with DF relaying under the practical assumption of imperfect SIC, where the UOWC channels are characterized by EGG distribution. We derived new analytical closed-form expressions for OPs and ECs and asymptotic expressions for the OPs and the DO . To gain more

insight, we investigated the influence of system parameters on performance. Consequently, we deduced that the increase in the level of air bubbles and/or temperature gradient leads to a degradation in the OPs and ECs performances, and the outage performance improves when implementing heterodyne detection compared to IM/DD. Moreover, we investigated the feasibility of obtaining an outage-optimal power allocation factor. Finally, we carried out a comparison with a benchmark system, from which we realize that our proposed system is suitable for UIoT applications. As a future work, we may study the a multi-underwater destination system with amplify and forward relay assuming imperfect channel state information.

Author Contributions: Conceptualization, A.A.A.E.-B.; Data curation, A.S. and M.E.; Formal analysis, A.S. and M.E.; Funding acquisition, I.S.A. and K.R.; Methodology, A.S. and M.E.; Project administration, B.M.E.; Software, A.S. and M.E.; Supervision, I.S.A., K.R. and B.M.E.; Validation, A.A.A.E.-B.; Writing—original draft, A.S. and M.E.; Writing—review & editing, K.R. and B.M.E. All authors have read and agreed to the published version of the manuscript.

Funding: This research received no external funding.

Institutional Review Board Statement: Not applicable.

Informed Consent Statement: Not applicable.

Conflicts of Interest: The authors declare no conflict of interest.

Appendix A

As the constraints in (29b) and (29c) are convex, consequently, we need to prove that the objective function (29a) is convex. Equation (14) is rewritten as

$$OP_{sys} = 1 - (1 - \theta_1 \tau)(1 - \theta_2 \tau^{\frac{1}{r}} - \theta_3 \tau^{\frac{ac}{r}})(1 - \theta_2 \tau_1^{\frac{1}{r}} - \theta_3 \tau_1^{\frac{ac}{r}}), \quad (A1)$$

where $\theta_1 = \frac{1}{\rho_s d^{-\nu}}$, $\theta_2 = \frac{w}{\lambda} (\frac{1}{\rho_R \mu_r})^{\frac{1}{r}}$, and $\theta_3 = \frac{1-w}{\Gamma(a+1)} (\frac{1}{b^r \rho_R \mu_r})^{\frac{ac}{r}}$.

As $\tau = \max(\tau_1, \tau_2)$, we can write (A1) as a piece-wise function based on the value of a_1 as

- For $\tau_1 > \tau_2$ or $\frac{\gamma_1}{1+\gamma_1} < a_1 < \frac{\gamma_1(1+\gamma_2)}{\gamma_1+\gamma_2+\gamma_1\gamma_2(1+\eta)}$, we rewrite (A1) as

$$OP_{sys} = 1 - (1 - \theta_1 \tau_1)(1 - \theta_2 \tau_1^{\frac{1}{r}} - \theta_3 \tau_1^{\frac{ac}{r}})^2 \quad (A2)$$

To differentiate OP_{sys} with respect to a_1 , we used the chain rule, $\frac{\partial OP_{sys}}{\partial a_1} = \frac{\partial OP_{sys}}{\partial \tau_1} \times \frac{\partial \tau_1}{\partial a_1}$, which result in

$$\begin{aligned} \frac{\partial OP_{sys}}{\partial a_1} = & -\frac{(1 + \gamma_1)\gamma_1}{(a_1(1 + \gamma_1) - \gamma_1)^2} [\theta_1(1 - \theta_2 \tau_1^{\frac{1}{r}} - \theta_3 \tau_1^{\frac{ac}{r}})^2 \\ & + 2(1 - \theta_1 \tau_1)(1 - \theta_2 \tau_1^{\frac{1}{r}} - \theta_3 \tau_1^{\frac{ac}{r}}) (\frac{\theta_2}{r} \tau_1^{\frac{1-r}{r}} + \frac{ac\theta_3}{r} \tau_1^{\frac{ac-r}{r}})], \end{aligned} \quad (A3)$$

which is always negative valued, this result indicates a monotonically decreasing function in this interval.

- For $\tau_1 < \tau_2$ or $\frac{\gamma_1(1+\gamma_2)}{\gamma_1+\gamma_2+\gamma_1\gamma_2(1+\eta)} < a_1 < \frac{1}{1+\eta\gamma_2}$, we rewrite (A1) as

$$OP_{sys} = 1 - \underbrace{(1 - \theta_1 \tau_2)}_{\psi_1} \underbrace{(1 - \theta_2 \tau_2^{\frac{1}{r}} - \theta_3 \tau_2^{\frac{ac}{r}})}_{\psi_2} \underbrace{(1 - \theta_2 \tau_1^{\frac{1}{r}} - \theta_3 \tau_1^{\frac{ac}{r}})}_{\psi_3}. \quad (A4)$$

To differentiate OP_{sys} with respect to a_1 in this interval, we use the chain rule, $\frac{\partial OP_{sys}}{\partial a_1} = \frac{\partial OP_{sys}}{\partial \tau_2} \times \frac{\partial \tau_2}{\partial a_1} + \frac{\partial OP_{sys}}{\partial \tau_1} \times \frac{\partial \tau_1}{\partial a_1}$, as τ_1 and τ_2 are independent. Using this rule, we obtain

$$\begin{aligned} \frac{\partial OP_{sys}}{\partial a_1} &= \theta_1 \frac{(1 + \eta\gamma_2)\gamma_2}{(1 - a_1(1 + \eta\gamma_2))^2} \psi_2 \psi_3 \\ &+ \left(\frac{\theta_2}{r} \tau_2^{\frac{1-r}{r}} + \frac{ac\theta_3}{r} \tau_2^{\frac{ac-r}{r}} \right) \frac{(1 + \eta\gamma_2)\gamma_2 \psi_1 \psi_3}{(1 - a_1(1 + \eta\gamma_2))^2} \\ &+ \left(\frac{\theta_2}{r} \tau_1^{\frac{1-r}{r}} + \frac{ac\theta_3}{r} \tau_1^{\frac{ac-r}{r}} \right) \frac{(1 + \gamma_1)\gamma_1 \psi_1 \psi_2}{(a_1(1 + \gamma_1) - \gamma_1)^2}, \end{aligned} \quad (A5)$$

which is clear that $\frac{\partial OP_{sys}}{\partial a_1}$ is always positive valued. This result indicates a monotonically increasing function in this interval. Now, we can observe that OP_{sys} is monotonically decreasing function in the interval $\frac{\gamma_1}{1 + \gamma_1} < a_1 < \frac{\gamma_1(1 + \gamma_2)}{\gamma_1 + \gamma_2 + \gamma_1\gamma_2(1 + \eta)}$ with the minimum value at the upper limit of this interval and monotonically increasing function in the interval $\frac{\gamma_1(1 + \gamma_2)}{\gamma_1 + \gamma_2 + \gamma_1\gamma_2(1 + \eta)} < a_1 < \frac{1}{1 + \eta\gamma_2}$ with the minimum at the lower limit of this interval. So, we conclude that OP_{sys} is a convex function with an optimal value at the turning point between the two intervals with outage-optimal power allocation of $a_1^* = \frac{\gamma_1(1 + \gamma_2)}{\gamma_1 + \gamma_2 + \gamma_1\gamma_2(1 + \eta)}$.

References

1. Saeed, N.; Celik, A.; Al-Naffouri, T.Y.; Alouini, M.S. Underwater optical wireless communications, networking, and localization: A survey. *Ad Hoc Netw.* **2019**, *94*, 101935. [\[CrossRef\]](#)
2. El-Banna, A.A.A.; Wu, K.; ElHalawany, B.M. Opportunistic Cooperative Transmission for Underwater Communication Based on the Water's Key Physical Variables. *IEEE Sens. J.* **2020**, *20*, 2792–2802. [\[CrossRef\]](#)
3. Aziz El-Banna, A.A.; Zaky, A.B.; ElHalawany, B.M.; Zhexue Huang, J.; Wu, K. Machine Learning Based Dynamic Cooperative Transmission Framework for IoUT Networks. In Proceedings of the 2019 16th Annual IEEE International Conference on Sensing, Communication, and Networking (SECON), Boston, MA, USA, 10–13 June 2019; pp. 1–9. [\[CrossRef\]](#)
4. Jain, M.; Sharma, N.; Gupta, A.; Rawal, D.; Garg, P. Performance Analysis of NOMA Assisted Underwater Visible Light Communication System. *IEEE Wirel. Commun. Lett.* **2020**, *9*, 1291–1294. [\[CrossRef\]](#)
5. Zedini, E.; Oubei, H.M.; Kammoun, A.; Hamdi, M.; Ooi, B.S.; Alouini, M.S. Unified Statistical Channel Model for Turbulence-Induced Fading in Underwater Wireless Optical Communication Systems. *IEEE Trans. Commun.* **2019**, *67*, 2893–2907. [\[CrossRef\]](#)
6. Ruby, R.; Zhong, S.; ElHalawany, B.M.; Luo, H.; Wu, K. SDN-Enabled Energy-Aware Routing in Underwater Multi-Modal Communication Networks. *IEEE/ACM Trans. Netw.* **2021**, *29*, 965–978. [\[CrossRef\]](#)
7. Li, S.; Yang, L.; da Costa, D.B.; Zhang, J.; Alouini, M.S. Performance Analysis of Mixed RF-UWOC Dual-Hop Transmission Systems. *IEEE Trans. Veh. Technol.* **2020**, *69*, 14043–14048. [\[CrossRef\]](#)
8. Li, S.; Yang, L.; da Costa, D.B.; Yu, S. Performance Analysis of UAV-Based Mixed RF-UWOC Transmission Systems. *IEEE Trans. Commun.* **2021**, *69*, 5559–5572. [\[CrossRef\]](#)
9. Ibrahim; Badrudduza, A.S.M.; Hossen, S.; Kundu, M.K.; Ansari, I.S. Enhancing Security of TAS/MRC Based Mixed RF-UOWC System with Induced Underwater Turbulence Effect. *arXiv* **2021**, arXiv:2105.09088.
10. Lou, Y.; Sun, R.; Cheng, J.; Nie, D.; Qiao, G. Secrecy Outage Analysis of Two-Hop Decode-and-Forward Mixed RF/UWOC Systems. *IEEE Commun. Lett.* **2021**, *26*, 989–993. [\[CrossRef\]](#)
11. Lei, H.; Zhang, Y.; Park, K.H.; Ansari, I.S.; Pan, G.; Alouini, M.S. Performance Analysis of Dual-Hop RF-UWOC Systems. *IEEE Photonics J.* **2020**, *12*, 7901915. [\[CrossRef\]](#)
12. Sarma, P.; Deka, R.; Anees, S. Performance Analysis of DF based Mixed Triple Hop RF-FSO-UWOC Cooperative System. In Proceedings of the 2020 IEEE 92nd Vehicular Technology Conference (VTC2020-Fall), Victoria, BC, Canada, 18 November–16 December 2020; pp. 1–5. [\[CrossRef\]](#)
13. Elsayed, M.; Samir, A.; El-Banna, A.A.; Li, X.; Elhalawany, B.M. When NOMA Multiplexing Meets Symbiotic Ambient Backscatter Communication: Outage Analysis. *IEEE Trans. Veh. Technol.* **2021**, *71*, 1026–1031. [\[CrossRef\]](#)
14. ElHalawany, B.M.; Jameel, F.; da Costa, D.B.; Dias, U.S.; Wu, K. Performance Analysis of Downlink NOMA Systems Over κ - μ Shadowed Fading Channels. *IEEE Trans. Veh. Technol.* **2020**, *69*, 1046–1050. [\[CrossRef\]](#)
15. Samir, A.; Elsayed, M.; El-Banna, A.A.; Wu, K.; Elhalawany, B.M. Performance of NOMA-Based Dual-hop Hybrid Powerline-Wireless Communication Systems. *IEEE Trans. Veh. Technol.* **2022**. [\[CrossRef\]](#)

16. Jain, M.; Sharma, N.; Gupta, A.; Rawal, D.; Garg, P. NOMA assisted underwater visible light communication system with full-duplex cooperative relaying. *Veh. Commun.* **2021**, *31*, 100359. [[CrossRef](#)]
17. Zhang, L.; Chen, Y.; Zhang, K.; Quan, J.; Li, Z.; Dong, Y. On Performance of Multiuser Underwater Wireless Optical Communication Systems. In Proceedings of the 2020 International Conference on Computing, Networking and Communications (ICNC), Big Island, HI, USA, 17–20 February 2020; pp. 1042–1046.
18. Khan, W.U.; Li, X.; Ihsan, A.; Ali, Z.; Elhalawany, B.M.; Sidhu, G.A.S. Energy Efficiency Maximization for beyond 5G NOMA-enabled Heterogeneous Networks. *Peer Peer Netw. Appl.* **2021**, *14*, 3250–3264. [[CrossRef](#)]
19. Aziz El-Banna, A.A.; Wu, K. *Machine Learning Modeling for IoUT Networks: Internet of Underwater Things*; Springer International Publishing: Cham, Switzerland, 2021.
20. Adamchik, V.S.; Marichev, O.I. The Algorithm for Calculating Integrals of Hypergeometric Type Functions and Its Realization in REDUCE System. In Proceedings of the international symposium on Symbolic and Algebraic Computation, Tokyo, Japan, 20–24 August 1990; Association for Computing Machinery: New York, NY, USA, 1990.
21. ElHalawany, B.M.; El-Banna, A.A.A.; Wu, K. Physical-Layer Security and Privacy for Vehicle-to-Everything. *IEEE Commun. Mag.* **2019**, *57*, 84–90. [[CrossRef](#)]
22. Rauniyar, A.; Engelstad, P.; Østerbø, O.N. Ergodic Capacity Performance of NOMA-SWIPT Aided IoT Relay Systems with Direct Link. In Proceedings of the 2020 18th International Symposium on Modeling and Optimization in Mobile, Ad Hoc, and Wireless Networks (WiOPT), Volos, Greece, 15–19 June 2020; pp. 1–8.
23. Gradshteyn, I.S.; Ryzhik, I.M.; Zwillinger, D.; Moll, V. *Table of Integrals, Series, and Products*, 8th ed.; Academic Press: Amsterdam, The Netherlands, 2014; ISBN 0123849330.